Support Vector Regression-Enabled Optimization Strategy of Dual Circularly-Polarized Shaped-Beam Reflectarray with Improved Cross-Polarization Performance

Daniel R. Prado, Parinaz Naseri, *Graduate Student Member, IEEE,* Jesús A. López-Fernández, Sean V. Hum, *Senior Member, IEEE,* and Manuel Arrebola, *Senior Member, IEEE*

***Abstract*—This work presents the optimization of a dual circular-polarized (CP) shaped-beam reflectarray with improved performance. To that end, the design methodology leverages surrogate models based on support vector regression (SVR) of the electromagnetic response of the constituent unit cell for a direct layout optimization of the antenna. The dual CP capability is achieved using a Linear Polarization (LP) Jerusalem cross integrated with an LP-to-CP polarization converter. A full description of the reflectarray analysis in CP is given. We also provide a missing demonstration in the literature of the fact that the direct coefficients in CP shape the copolar pattern of the corresponding polarization. This is applied to the optimization of a dual CP reflectarray with an isoflux pattern, achieving a reduction of more than 9 dB in the crosspolar pattern.**

***Index Terms*—Reflectarray antennas, dual circular polarization, machine learning, support vector regression, surrogate models, shaped-beam antenna, crosspolar optimization.**

I. Introduction

CIRCULAR polarization (CP) is of great interest for communication systems for several reasons [1]. For instance, CP is particularly effective at minimizing multipath interference since the polarization of the reflected signal becomes inverted and the CP antenna will reject it [2]. In addition, unlike linear polarized (LP) antennas, there is no polarization mismatch as a result of a misalignment between the receiving and transmitting antennas in CP. Another advantage is that the CP wave does not suffer from the Faraday rotation effect as the LP does.

For high-gain applications that require CP, reflectarray antennas have proven to be useful [3]. In addition to their low mass and low profile, they allow easy focusing of the beam to any desired direction by simply adjusting the phase-shift of the reflecting elements. In addition, passive reflectarrays are easy to fabricate using printed circuit board technology. One of the first demonstrators of a CP reflectarray was based on rotated microstrip patches [4]. Since then, many CP reflectarrays have been developed that are single-band single-CP [5], single-band dual-CP [6], dual-band single-CP [7] and more recently in dual-band dual-CP [8]–[12]. CP operation may be achieved using CP feeds and the variable rotation technique [4], [5], [9]–[11], in which the phase-shift introduced by the element working in CP is proportional to twice the angle of rotation. The required phase shift can also be achieved by varying the lengths of arc-shaped stubs aperture-coupled to a patch [6], [12]. It may also be achieved by employing a 45°- or 135°-directed LP feed with regard to the reflectarray to decompose the impinging LP wave into two components with equal magnitude [7], [8].

In this regard, much effort has been devoted to develop unit cells that provide the required characteristics. For instance, in [9] a split hexagonal-loop with a dipole inside is employed, in which each structure can be rotated independently to achieve control of the phase-shift in two bands. In [10] a dual-band dual-LP reflectarray element in conjunction with a dual-band LP-to-CP polarizer is employed. The unit cell in [11] is composed of two stacked orthogonal sets of three parallel dipoles and two symmetrical arcs. In [12] the dual-wideband dual-CP performance is achieved by interleaving a circular patch with a slotted cross that is aperture-coupled to short-ended arc-shaped delay lines with variable length.

Reflectarrays may be designed to either collimate a beam or to produce a shaped beam. In this regard, a common feature of all the works mentioned above is that the designed reflectarrays radiate a collimated beam. This is relatively easy to achieve since analytical approaches are available [3]. In addition, the synthesis of shaped-beam reflectarrays in LP or dual-LP has been widely studied [3]. However, few works have

This work was supported in part by the Ministerio de Ciencia, Innovación y Universidades under project IJC2018-035696-I; by the Ministerio de Ciencia e Innovación and the Agencia Estatal de Investigación within project ENHANCE-5G (PID2020-114172RB-C21 / AEI / 10.13039/501100011033); by Gobierno del Principado de Asturias under project AYUD/2021/51706; and by the Natural Sciences and Engineering Research Council of Canada (NSERC) at the University of Toronto.

D. R. Prado, J. A. López-Fernández and M. Arrebola are with the Department of Electrical Engineering, Group of Signal Theory and Communications Universidad de Oviedo, Gijón 33203, Spain (e-mail: drprado@uniovi.es; jelofer@uniovi.es; arrebola@uniovi.es).

P. Naseri and S. V. Hum are with the Edward S. Rogers Sr. Department of Electrical and Computer Engineering, University of Toronto, Toronto, ON M5S 3G4, Canada (e-mail: parinaz.naseri@utoronto.ca; sean.hum@utoronto.ca).

Color versions of one or more of the figures in this paper are available online at http://ieeexplore.ieee.org.

Digital Object Identifier XX.XXXX/XXX.XXXX.XXXXXXX

dealt with shaped-beam reflectarrays working in CP. In [13] a dual-band shaped-beam single-CP reflectarray is designed using a phase-only synthesis (POS) based on particle swarm optimization. In [14] a single CP contoured-beam reflectarray to provide coverage to the Russian Federation is designed using the intersection approach (IA) algorithm for a POS. In [15] a single-CP contoured-beam reflectarray for space applications was designed performing a direct layout optimization. However, these works do not provide a convenient description of the synthesis procedure in CP or the relation between the coefficients in CP and the common reflectarray analysis formulation in LP, as employed in [13]. More importantly, manipulating and improving the cross-polarization level is yet to be addressed in CP shaped-beam reflectarrays.

In this work, an optimization of a dual-CP shaped-beam reflectarray with improved performance is presented. To that end, a strategy for the analysis, design and direct layout optimization of dual-CP reflectarrays is provided. A detailed formulation of the analysis of dual-CP reflectarrays is developed and then particularized for POS. A demonstration is given of the fact that the direct coefficients in CP shape the copolar pattern of the corresponding polarization, provided a good performance of the feed and unit cell. Although this was already shown for LP [16], it is a non-trivial task to demonstrate it for CP since no direct expression of the far fields as a function of the CP reflection coefficients is available in the literature. In addition, the direct use of commercial general-purpose electromagnetic analysis software is not viable for direct reflectarray optimization due to the excessive time cost involved. Thus, support vector regression (SVR) surrogate models of the unit cell are employed in the optimization of the antenna. A direct layout optimization employing the generalized IA (GIA) [17] is carried out, obtaining a shaped-beam reflectarray with an isoflux pattern for global Earth coverage with improved cross-polarization performance.

The paper is organized as follows. Section II includes the CP formulation of reflectarray antennas. In Section III, the SVR modelling of the unit cell is described. Section IV presents the optimization of a dual-CP shaped-beam reflectarray. Finally, Section V contains the conclusions.

II. Circular Polarization Formulation for Reflectarray Optimization

A. Field at the Aperture

Fig. 1 shows a sketch of the reflectarray single offset-fed configuration that is considered in this work. The reflectarray coordinate system is $(\hat{x}, \hat{y}, \hat{z})$. The feed illuminates the reflectarray generating a tangential incident field on the reflectarray surface, which is expressed in Cartesian basis as[1]:

$$\vec{E}^{\mathrm{LP}}_{\mathrm{inc}}(x, y) = E_{\mathrm{inc},x}\hat{x} + E_{\mathrm{inc},y}\hat{y}. \tag{1}$$

The dependence on the coordinates (x, y) of the field components has been removed from (1) and subsequent equations to alleviate the notation. Then, the tangential reflected field

[1]The notation LP in this subsection denotes Cartesian basis

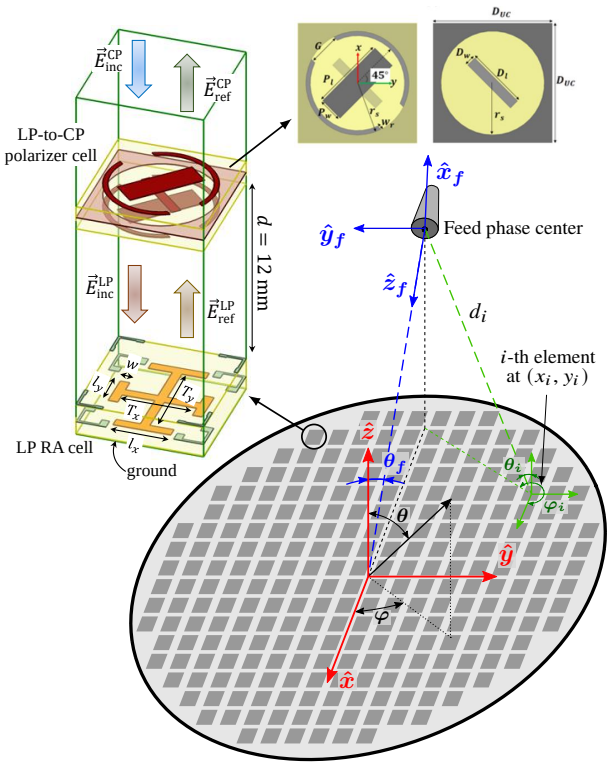

Fig. 1. Sketch of a generic reflectarray in single-offset configuration for which the CP POS formulation is developed, showing the reflectarray coordinate system $(\hat{x}, \hat{y}, \hat{z})$ and the feed coordinate system $(\hat{x}_f, \hat{y}_f, \hat{z}_f)$. The unit vectors are related as follows: $\hat{x} = \hat{x}_f \cos\theta_f + \hat{z}_f \sin\theta_f$, $\hat{y} = -\hat{y}_f$, $\hat{z} = \hat{x}_f \sin\theta_f - \hat{z}_f \cos\theta_f$. The inset shows the employed unit cell with dual-CP capability employed in this work. By varying T_x and T_y, a phase-shift is achieved in $\angle\rho_{rr}$ and $\angle\rho_{ll}$, respectively.

at the reflectarray aperture can be obtained from the incident field in (1) and the matrix of reflection coefficients:

$$\vec{E}^{\mathrm{LP}}_{\mathrm{ref}}(x, y) = \boldsymbol{R}_{\mathrm{cart}}\, \vec{E}^{\mathrm{LP}}_{\mathrm{inc}}(x, y), \tag{2}$$

where $\boldsymbol{R}_{\mathrm{cart}}$ is the matrix of reflection coefficients in Cartesian basis which relates the $\hat{x}$ and $\hat{y}$ components of the incident and reflected tangential fields:

$$\boldsymbol{R}_{\mathrm{cart}} = \begin{pmatrix} \rho_{xx} & \rho_{xy} \\ \rho_{yx} & \rho_{yy} \end{pmatrix}, \tag{3}$$

where ρ_{xx} and ρ_{yy} are known as the direct (reflection) coefficients, while ρ_{xy} and ρ_{yx} are the cross-coefficients.

In LP, the phases of ρ_{xx} and ρ_{yy} give the phase-shift distribution that shape the copolar pattern for X and Y linear polarizations, respectively [16]. However, this is not the case for CP. In order to perform a CP optimization, we need to deduce an expression for two reflection coefficients, ρ_{rr} and ρ_{ll}, that shape the copolar pattern for right-hand CP (RHCP) and left-hand CP (LHCP), respectively. To that end, we start by defining the matrix of reflection coefficients in a CP basis:

$$\boldsymbol{R}_{\mathrm{circ}} = \begin{pmatrix} \rho_{rr} & \rho_{rl} \\ \rho_{lr} & \rho_{ll} \end{pmatrix}. \tag{4}$$

Similarly to $\boldsymbol{R}_{\mathrm{cart}}$, ρ_{rr} and ρ_{ll} are the direct coefficients, while ρ_{rl} and ρ_{lr} are the cross-coefficients. $\boldsymbol{R}_{\mathrm{circ}}$ relates the

components in CP of the reflected and incident fields:

$$\vec{E}^{\mathrm{CP}}_{\mathrm{ref}}(x,y) = \boldsymbol{R}_{\mathrm{circ}}\,\vec{E}^{\mathrm{CP}}_{\mathrm{inc}}(x,y), \tag{5}$$

where:

$$\vec{E}^{\mathrm{CP}}_{\mathrm{ref}}(x,y) = E_{\mathrm{ref},r}\hat{r} + E_{\mathrm{ref},l}\hat{l}, \tag{6}$$

and $\hat{r}$ and $\hat{l}$ are the CP unit vectors on the reflectarray surface defined as $\hat{r} = (\hat{x} - j\hat{y})/\sqrt{2}$ and $\hat{l} = (\hat{x} + j\hat{y})/\sqrt{2}$ according to the geometry defined in Fig. 1. It is straightforward to obtain the reflected CP components in terms of the reflected LP components as:

$$\begin{aligned} E_{\mathrm{ref},r} &= \vec{E}^{\mathrm{LP}}_{\mathrm{ref}} \cdot \hat{r}^* = (E_{\mathrm{ref},x} + jE_{\mathrm{ref},y})/\sqrt{2}, \\ E_{\mathrm{ref},l} &= \vec{E}^{\mathrm{LP}}_{\mathrm{ref}} \cdot \hat{l}^* = (E_{\mathrm{ref},x} - jE_{\mathrm{ref},y})/\sqrt{2}. \end{aligned} \tag{7}$$

In (7), the asterisk represents the complex conjugate. (Please notice that $\hat{r}\cdot\hat{r}^* = \hat{l}\cdot\hat{l}^* = 1$ and $\hat{r}\cdot\hat{l}^* = \hat{l}\cdot\hat{r}^* = 0$.) Since the propagation direction of the incident and the reflected fields are reversed, we can define:

$$\vec{E}^{\mathrm{CP}}_{\mathrm{inc}}(x,y) = E_{\mathrm{inc},r}\hat{r}_{\mathrm{inc}} + E_{\mathrm{inc},l}\hat{l}_{\mathrm{inc}}, \tag{8}$$

where $\hat{r}_{\mathrm{inc}} = \hat{l}$ and $\hat{l}_{\mathrm{inc}} = \hat{r}$. Please notice that from Fig. 1 that $\hat{y} = -\hat{y}_f$ and that the projection of $\hat{x}_f$ onto the reflectarray surface is aligned with $\hat{x}$. Then we have:

$$\begin{aligned} E_{\mathrm{inc},r} &= \vec{E}^{\mathrm{LP}}_{\mathrm{inc}} \cdot \hat{r}^*_{\mathrm{inc}} = (E_{\mathrm{inc},x} - jE_{\mathrm{inc},y})/\sqrt{2}, \\ E_{\mathrm{inc},l} &= \vec{E}^{\mathrm{LP}}_{\mathrm{inc}} \cdot \hat{l}^*_{\mathrm{inc}} = (E_{\mathrm{inc},x} + jE_{\mathrm{inc},y})/\sqrt{2}. \end{aligned} \tag{9}$$

By substituting (9) into (5) we obtain two equations of the components of $\vec{E}^{\mathrm{CP}}_{\mathrm{ref}}$ in terms of $\boldsymbol{R}_{\mathrm{circ}}$ and the incident field in a Cartesian basis. Then, by substituting the expanded version of (2) into (7), we obtain another two equations of the components $\vec{E}^{\mathrm{CP}}_{\mathrm{ref}}$ in terms of $\boldsymbol{R}_{\mathrm{cart}}$ and the incident field in Cartesian basis. With these two sets of equations, we can relate the two components—$\hat{x}$ and $\hat{y}$—of $\vec{E}^{\mathrm{CP}}_{\mathrm{ref}}$ with the two components of $\vec{E}^{\mathrm{LP}}_{\mathrm{inc}}$, one set using $\boldsymbol{R}_{\mathrm{circ}}$ and the other set using $\boldsymbol{R}_{\mathrm{cart}}$. In this way, by equating each component, we obtain a system of four equations relating $\boldsymbol{R}_{\mathrm{circ}}$ with $\boldsymbol{R}_{\mathrm{cart}}$. After solving this system of equations we obtain:

$$\boldsymbol{\rho}_{\mathrm{LP}} = \boldsymbol{M}\boldsymbol{\rho}_{\mathrm{CP}}, \tag{10a}$$

$$\boldsymbol{\rho}_{\mathrm{CP}} = \boldsymbol{M}^{-1}\boldsymbol{\rho}_{\mathrm{LP}}, \tag{10b}$$

with $\boldsymbol{\rho}_{\mathrm{LP}} = (\rho_{xx}, \rho_{xy}, \rho_{yx}, \rho_{yy})^T$, $\boldsymbol{\rho}_{\mathrm{CP}} = (\rho_{rr}, \rho_{rl}, \rho_{lr}, \rho_{ll})^T$, $(\cdot)^T$ is the transpose of a vector, and M^{-1} is the inverse of:

$$\boldsymbol{M} = \frac{1}{2}\begin{pmatrix} 1 & 1 & 1 & 1 \\ -j & j & -j & j \\ -j & -j & j & j \\ -1 & 1 & 1 & -1 \end{pmatrix}. \tag{11}$$

Equation (10) allows to change the reflection coefficients from Cartesian basis (i.e., LP) to a circular polarization basis and vice versa. When applied to POS in CP, reflection coefficients in (10a) need to be employed since the spectrum functions (see Subsection II-B) in the usual formulation are defined in Cartesian basis as in [3]. However, the relation between the reflection coefficients in CP basis (i.e., $\boldsymbol{R}_{\mathrm{circ}}$) and the far-field has not yet been established. In particular, it is not evident whether the copolar patterns in CP mainly depend on the direct coefficients. The truthfulness of this hypothesis is necessary to perform POS in CP and it will be verified in the following subsections.

B. Far-Field Formulation

The far-field $\vec{E}_{\mathrm{ff}}$ can be defined as [2]:

$$\vec{E}_{\mathrm{ff}}(r,\theta,\varphi) = E_\theta\hat{\theta} + E_\varphi\hat{\varphi}. \tag{12}$$

The dependence on the coordinates (r,θ,φ) of the far-field components has been removed from (12) and subsequent equations to alleviate notation. The RHCP (r) and LHCP (l) components may be obtained as:

$$\begin{aligned} E_{\mathrm{ff},r} &= \vec{E}_{\mathrm{ff}} \cdot \hat{r}^*_{\mathrm{ff}} = \left(E_\theta + jE_\varphi\right)/\sqrt{2}, \\ E_{\mathrm{ff},l} &= \vec{E}_{\mathrm{ff}} \cdot \hat{l}^*_{\mathrm{ff}} = \left(E_\theta - jE_\varphi\right)/\sqrt{2}. \end{aligned} \tag{13}$$

Here, $\hat{r}_{\mathrm{ff}}$ and $\hat{l}_{\mathrm{ff}}$ are the far field CP unit vectors defined as $\hat{r}_{\mathrm{ff}} = (\hat{\theta} - j\hat{\varphi})/\sqrt{2}$ and $\hat{l}_{\mathrm{ff}} = (\hat{\theta} + j\hat{\varphi})/\sqrt{2}$.

By defining the spectrum function of the electric field in circular polarization as:

$$P_{r/l} = \iint_S E_{\mathrm{ref},r/l}(x,y)\exp(jk_0(ux+vy))dxdy, \tag{14}$$

where S is the reflectarray surface, k_0 is the free-space wavenumber and $u = \sin\theta\cos\varphi$, $v = \sin\theta\sin\varphi$, the far field CP components may be expressed as:

$$\begin{aligned} E_{\mathrm{ff},r} &= C_1P_r + C_2P_l, \\ E_{\mathrm{ff},l} &= C_3P_r + C_4P_l. \end{aligned} \tag{15}$$

In this way, the CP components of the far field have been expressed as a function of the CP spectrum functions $P_{r/l}$. Details on the derivation of (15) as well as the definition of C_1, C_2, C_3, C_4 may be consulted in the Appendix.

The next step is to apply the developed formulation to POS.

C. Application to Phase-Only Synthesis

The goal of the POS in CP is to obtain the phase distribution of the direct coefficients, ρ_{rr} and ρ_{ll}, that shape the copolar pattern for the RHCP and LHCP, respectively. However, according to (15), both CP components of the far-field depend on both spectrum functions in CP and thus on both ρ_{rr} and ρ_{ll}. To prove that the copolar components of the far field mainly depend on the corresponding reflection coefficient for each polarization, we introduce the notation for dual CP. Expanding (5):

$$\begin{aligned} \vec{E}^{R/L}_{\mathrm{ref},r} &= \rho_{rr}E^{R/L}_{\mathrm{inc},r}\hat{r} + \rho_{rl}E^{R/L}_{\mathrm{inc},l}\hat{l}, \\ \vec{E}^{R/L}_{\mathrm{ref},l} &= \rho_{lr}E^{R/L}_{\mathrm{inc},r}\hat{r} + \rho_{ll}E^{R/L}_{\mathrm{inc},l}\hat{l}, \end{aligned} \tag{16}$$

where the R and L superscripts indicate the polarization of the reflectarray for RHCP or LHCP, respectively. For a CP reflectarray fed by a CP feed and depending on the polarization, the following conditions will be assumed:

$$\begin{aligned} \text{RHCP: } &|E^R_{\mathrm{inc},r}| \gg |E^R_{\mathrm{inc},l}| \text{ and } |\rho_{rr}| \gg |\rho_{rl}| \Rightarrow \\ &|\rho_{rr}E^R_{\mathrm{inc},r}| \gg |\rho_{rl}E^R_{\mathrm{inc},l}| \text{ and } |E^R_{\mathrm{ref},r}| \gg |E^R_{\mathrm{ref},l}|. \end{aligned} \tag{17}$$

$$\begin{aligned} \text{LHCP: } &|E^L_{\mathrm{inc},l}| \gg |E^L_{\mathrm{inc},r}| \text{ and } |\rho_{ll}| \gg |\rho_{lr}| \Rightarrow \\ &|\rho_{ll}E^L_{\mathrm{inc},l}| \gg |\rho_{lr}E^L_{\mathrm{inc},r}| \text{ and } |E^L_{\mathrm{ref},l}| \gg |E^L_{\mathrm{ref},r}|. \end{aligned} \tag{18}$$

The fulfilment of these conditions depends on the good performance of the CP feed and unit cell. Then, the reflected tangential electric field may be approximated by

$$\begin{aligned}\vec{E}^R_{\text{ref}} &\approx \rho_{rr} E^R_{\text{inc},r}\hat{r},\\ \vec{E}^L_{\text{ref}} &\approx \rho_{ll} E^L_{\text{inc},l}\hat{l}.\end{aligned} \tag{19}$$

Using this notation, the copolar (CO) patterns from (15) for both circular polarizations are

$$\begin{aligned}\text{RHCP (CO): } E^R_{\text{ff},r} &= C_1 P^R_r + C_2 P^R_l,\\ \text{LHCP (CO): } E^L_{\text{ff},l} &= C_3 P^L_r + C_4 P^L_l.\end{aligned} \tag{20}$$

The approximation in (19) implies that $P^R_l \approx 0$ and $P^L_r \approx 0$, so we finally have

$$\begin{aligned}\text{RHCP: } E^R_{\text{ff},r} &\approx C_1 P^R_r,\\ \text{LHCP: } E^L_{\text{ff},l} &\approx C_4 P^L_l.\end{aligned} \tag{21}$$

By virtue of (19), P_r only depends on ρ_{rr} and P_l on ρ_{ll}. Hence, it is proven that the copolar patterns in CP are mainly shaped by the corresponding reflection coefficient, given that the conditions in (17) and (18) are fulfilled.

The POS analysis assumes an ideal phase-shifter with no losses ($|\rho_{rr}| = |\rho_{ll}| = 1$) and no cross-polarization ($\rho_{rl} = \rho_{lr} = 0$). In such case, (10a) is simplified to:

$$\begin{aligned}\rho_{xx} &= \ \ 0.5(\ \ \rho_{rr} + \rho_{ll}),\\ \rho_{xy} &= j0.5(-\rho_{rr} + \rho_{ll}),\\ \rho_{yx} &= j0.5(-\rho_{rr} + \rho_{ll}),\\ \rho_{yy} &= \ \ 0.5(-\rho_{rr} - \rho_{ll}).\end{aligned} \tag{22}$$

Once the reflection coefficients are obtained in Cartesian basis, the spectrum functions in (26) can be obtained, and from there, the far-field in (13). Thus, it is possible to use the usual LP formulation to carry out the POS in CP by using (22). Please note that since the POS is carried out in CP, the POS analysis simplification is applied to $\boldsymbol{R}_{\text{circ}}$. But by virtue of (22), all four coefficients of $\boldsymbol{R}_{\text{cart}}$ are needed.

D. Limitations of the POS in Dual-CP Reflectarrays

The correct performance of the POS relies upon the fulfilment of (17) for RHCP and (18) for LHCP. A careful analysis of these simplifications shows that they depend on the good performance of both the feed and unit cell. On the one hand, the feed needs to provide a good polarization purity on the reflectarray surface. This is the assumption of $|E^R_{\text{inc},r}| \gg |E^R_{\text{inc},l}|$ for RHCP and $|E^L_{\text{inc},l}| \gg |E^L_{\text{inc},r}|$ for LHCP.

On the other hand, the unit cell has to provide a response such that ρ_{rl} and ρ_{lr} present a low magnitude compared to ρ_{rr} and ρ_{ll}. In this regard, the power balance equations [18] establish that, in the absence of losses, a low magnitude in the direct coefficients will translate to higher cross-coefficient values. Since the magnitude of the direct coefficients is directly related to the achievable gain of the antenna, it is desired to use a unit cell that provides low losses and low cross-polarization.

If the approximations in (17) and (18) fail, either due to the feed, unit cell or both, the consequence will be a distorted copolar pattern after a layout is obtained from the synthesized phase-shift distributions. In the case of collimated beams, this means a lower gain (i.e., lower efficiency of the antenna), and in the case of shaped beams, a distortion of the pattern that will prevent it from complying with the specifications set in the POS. In such case, a direct optimization of the layout, considering the actual response of the unit cell, is required to not only correctly shape the copolar beam, but also to minimize the crosspolar pattern since this time no simplifications on the incident field and reflection coefficients are assumed. Despite this shortcoming of the POS, it may still be interesting to perform an initial POS to obtain a suitable starting point for the direct layout optimization, since a distorted shaped-beam pattern may be closer to the solution than another pattern, such as a collimated beam.

Finally, it is worth mentioning that the limitations discussed here also apply to POS in dual LP.

III. SVR MODELLING OF THE UNIT CELL

A. Description of the Unit Cell

In order to achieve dual-CP capability, an appropriate unit cell must be employed. For this work, we use the unit cell shown in Fig. 1 that was previously proposed and validated through measurements of a prototype in [10]. The unit cell consists of an LP reflectarray unit cell (LP RA cell) realized using Jerusalem crosses and an LP-to-CP polarizer. The polarizer transforms an incident CP wave into an LP wave, whose phase is shifted by the LP RA cell and reflected back. Then, the reflected LP wave is converted back to a CP wave by the polarizer. The whole unit cell can adjust the phase of each CP incident wave independently. While the unit cell operates in two frequencies of Ka-band satellite communication providing dual-band dual-CP capabilities [10], here for the purpose of showing the proposed optimization method, the process is performed only at 18.5 GHz in the lower band.

In the lower band, the largest Jerusalem cross at the center of the LP RA controls the phase shift of the reflected wave. Thus, the optimizing variables will be the arm lengths of this Jerusalem cross, T_x and T_y, as shown in Fig. 1. The range of variation of these variables is $[2.6, 3.7]$ mm, providing a phase-shift range slightly larger than 300° across several angles of incidence. The other dimensions of the unit cell are $l_{x/y} = T_{x/y} - 1.6\,\text{mm}$ and $w = 0.4\,\text{mm}$. In addition, the periodicity is set to 5.3 mm in both dimensions, and the substrate is comprised of two layers of Rogers RT/Duroid 5880 ($\varepsilon = 2.2$, $\tan\delta = 0.0009$), with a thickness of 0.508 mm for the bottom layer and 0.787 mm for the top layer. The characteristics of the polarizer are fixed and they are, referring to Fig. 1: $D_l = 2.7\,\text{mm}$, $D_w = 0.45\,\text{mm}$, $D_{\text{uc}} = 5.3\,\text{mm}$, $G = 1.4\,\text{mm}$, $P_l = 3.3\,\text{mm}$, $P_w = 1.1\,\text{mm}$, $r_s = 2.3\,\text{mm}$, $w_r = 0.2\,\text{mm}$.

B. Generation of the Database

The unit cell is simulated in Ansys HFSS [19] using a Floquet port excitation and in periodic boundary conditions under the following set of angles of incidence: $\theta = \{0°, 5°, 10°, \ldots, 35°\}$, $\varphi = \{0°, \pm 15°, \pm 30°, \pm 45°, \pm 60°\}$.

Thus, a total of 64 (θ, φ) pairs are employed, in which $\theta = 0°$ is only considered in combination with $\varphi = 0°$.

For each angle of incidence (θ, φ), 529 samples are generated at a single frequency, 18.5 GHz. It has to be noted that this is a very time consuming process. In an Intel i9-9900 CPU working at 3.1 GHz and with 32 GB of memory, each sample takes approximately three minutes to be simulated. Thus, 71 days are necessary to obtain all the required samples if one instance of HFSS is used at a time. However, once all the samples have been acquired, they can be employed to design any reflectarray with this unit cell characteristics.

C. Support Vector Regression Model Training

The database is employed to train surrogate models that efficiently provide a very accurate estimation of the reflection coefficients during the reflectarray optimization phases. This is done employing support vector regression (SVR) where the input space comprises the cell dimensions, $\vec{x} = (T_x, T_y) \in \chi$, and the output spaces consist of the reflection coefficients.

We model the reflection coefficients in Cartesian basis. In addition, SVR is conceived to calculate real-valued functions, though the reflection coefficients are complex-valued. As a consequence, to model ρ_{xx}, ρ_{xy}, ρ_{yx}, and ρ_{yy} for each angle of incidence, we need to obtain at least eight regression functions: one model for the real part and another one for the imaginary part of each reflection coefficient. In contrast with previous works [20], the accuracy of the estimation for the direct coefficients magnitude does not benefit from modeling them directly. In the rest of this subsection, the symbol ρ denotes indistinctly a reflection coefficient in (3), or its real or imaginary parts.

We use a cross-validation procedure to obtain the surrogate models. Thus, the set of $N = 529$ generated samples is divided into three groups: training ($N_r = 371 \approx 0.7N$), validation ($N_v = 79 \approx 0.15N$), and test ($N_t = 79 \approx 0.15N$). The training data is used to obtain the regression function $f(\vec{x})$ with the LibSVM library [21] that allows the estimation of ρ, $\widetilde{\rho}$, for any new input $\vec{x} \in \chi$ such that:

$$\tilde{\rho} = f(\vec{x}) = \sum_{i=1}^{N_s} \left[\left(\alpha_i^- - \alpha_i^+ \right) K(\vec{x}_i, \vec{x}) \right] + b, \qquad (23)$$

where N_s is the number of support vectors; α_i^- and α_i^+ are the optimal Lagrange multipliers; $\vec{x}_i$ are the support vectors; $K(\cdot, \cdot)$ is the (Gaussian) kernel function, and b is the offset. The accuracy of the model is eventually determined by its error over the test set that is not used in any part of the training process. For a detailed explanation, the reader is referred to earlier work [22].

This training procedure is very fast. In the present case, each surrogate model takes an average time of 6.2 s and the global average test error is −22.1 dB, considering all reflection coefficients across all angles of incidence. A summary of the mean test error and mean training time for each coefficient can be consulted in Table I. From the output of the SVR models, the coefficients in CP basis are readily obtained using (10b).

Table I
MEAN TEST ERROR AND TRAINING TIME OF THE SVR MODELS ACROSS ALL CONSIDERED ANGLES OF INCIDENCE AT 18.5 GHZ.

	Mean test error (dB)	Mean training time (s)
$\mathrm{Re}\{\rho_{xx}\}$	−20.3	7.4
$\mathrm{Im}\{\rho_{xx}\}$	−22.4	7.3
$\mathrm{Re}\{\rho_{xy}\}$	−25.7	5.8
$\mathrm{Im}\{\rho_{xy}\}$	−21.3	6.6
$\mathrm{Re}\{\rho_{yx}\}$	−25.8	5.4
$\mathrm{Im}\{\rho_{yx}\}$	−21.2	6.4
$\mathrm{Re}\{\rho_{yy}\}$	−20.3	6.9
$\mathrm{Im}\{\rho_{yy}\}$	−21.9	7.1
Global	−22.1	6.6

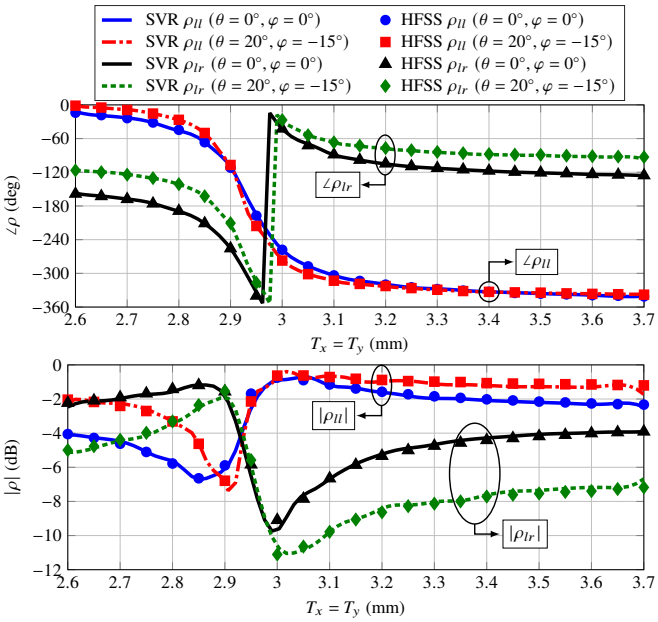

Fig. 2. Comparison between the SVR surrogate model simulations in the prediction of the reflection coefficients and HFSS simulations for the direct coefficient ρ_{ll} and cross-coefficient ρ_{lr} in phase (top) and magnitude (bottom) for normal and oblique incidence at 18.5 GHz.

D. Reflection coefficients

Fig. 2 shows a comparison between the SVR-based and HFSS simulations of two reflection coefficients, ρ_{ll} and ρ_{lr}, in magnitude and phase for normal and oblique incidence, showing a high degree of accuracy. Similar accuracy has been obtained for other reflection coefficients and angles of incidence.

As shown in Fig. 2, this unit cell is able to provide slightly more than 300° of phase-shift under oblique incidence. Thus, the POS will have to take into account this limitation for a subsequent layout design step. Moreover, from the magnitude response of the direct coefficients, we can see that there is a resonance with high losses corresponding with the maximum variation in the phase-shift curve. This means that the antenna will present high losses in the copolar pattern when compared to an analysis assuming ideal phase-shifters. Furthermore, the cross-polarization introduced by the unit cell is also very high, as seen in the magnitude of the cross-coefficient. This means that the limitations of the POS discussed in Section II-D will

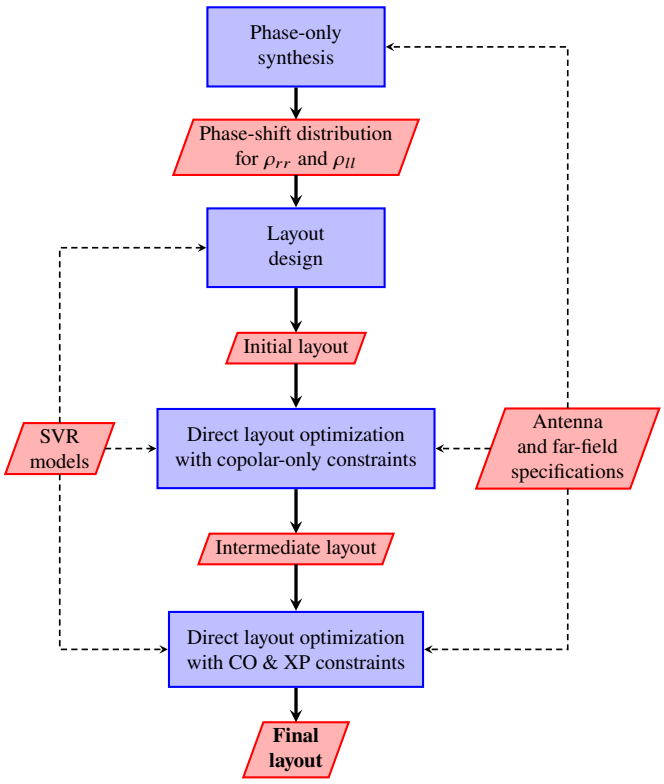

Fig. 3. Flowchart of the dual-CP shaped-beam reflectarray design process.

come into play distorting the radiation pattern.

IV. Optimization of a Dual-CP Reflectarray with Improved Cross-Polarization Performance

A. Antenna and Far-field Specifications

We consider a reflectarray in single-offset configuration as shown in Fig. 1, comprised of 1 024 elements in a regular grid of 32×32. The unit cell and its characteristics are detailed in Section III-A. As feed, a spherical wave expansion (SWE) model of a custom feed horn is employed. The phase-center of the feed is placed at $(-79.2, 0.0, 182.6)$ mm with respect to the reflectarray center, generating an average edge illumination taper of -14 dB at the working frequency, 18.5 GHz.

For the far-field, an isoflux pattern is considered. It comprises a coverage area with an allowable ripple, a transition zone and a non-coverage area given by the side lobe level (SLL). The atenuation curve for the coverage area is defined by the Friis equation [23]. For this work, we consider a 1 dB-allowable ripple in the coverage area and side lobe levels of -19 dB with regard to the maximum gain. The antenna is assumed to be placed in a satellite in geostationary orbit to provide global Earth coverage.

B. Phase-only Synthesis

Fig. 3 shows a flowchart of the whole design process. It is divided into several stages to facilitate convergence towards a suitable solution. The first step is to perform a POS to obtain the phase-shift distributions for ρ_{rr} and ρ_{ll} that provide the desired isoflux pattern in dual CP. To that end, the GIA for

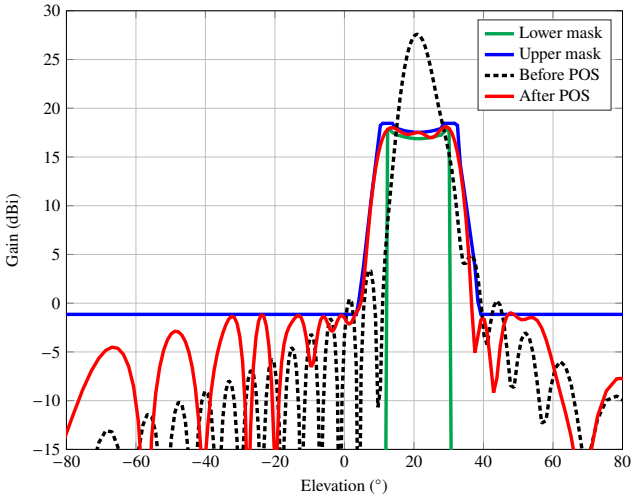

Fig. 4. Main cut in elevation of the copolar pattern for RHCP before (pencil beam) and after (isoflux pattern) the POS at 18.5 GHz.

POS [20] is adapted to employ the formulation developed in Section II. As a starting point for the POS, a collimated beam pointing at the centre of the isoflux pattern is used. In addition, the POS will take into account the phase-shift restriction of the unit cell by limiting $\angle\rho_{rr}$ and $\angle\rho_{rr}$ to a range of 300°.

Fig. 4 shows the main cuts of the simulated radiation patterns before and after the POS assuming ideal phase-shifters. As can be seen, the isoflux pattern perfectly complies with the imposed restrictions by the mask templates. Similar results were obtained for LHCP.

C. Layout Design

Once the desired phase-shift distributions have been obtained for $\angle\rho_{rr}$ and $\angle\rho_{ll}$, the next step is to obtain a layout, that is, to find the dimensions of the Jerusalem crosses such that they provide the appropriate phase-shift for each polarization. This process consists of three steps which have been described previously [20] but will be summarized here for completeness. First, and for each reflectarray element, two phase-shift tables are generated independently for each polarization. Then, the lengths of the arms of the Jerusalem cross are adjusted using a linear equation. Finally, the Newton-Raphson (N-R) method is employed to adjust both dimensions at the same time. After the layout is obtained, it can be simulated using the SVR models to obtain the reflected tangential field with no simplifications on the matrix of reflection coefficients, and from there the radiation pattern.

Fig. 5 shows the elevation cut of the copolar and crosspolar components produced by the simulated layout for both RHCP and LHCP. Two things stand out. First, the copolar pattern is very distorted, with lower gain than the one shown in Fig. 4. Second, the crosspolar pattern level is very high, even more than the copolar pattern. These two issues can be explained by the electromagnetic response of the unit cell, which is very different from an ideal phase-shifter. High losses in the magnitude of the direct coefficients means that the gain will drop significantly, while a high magnitude of the cross-coefficients means that the crosspolar pattern gain will be very

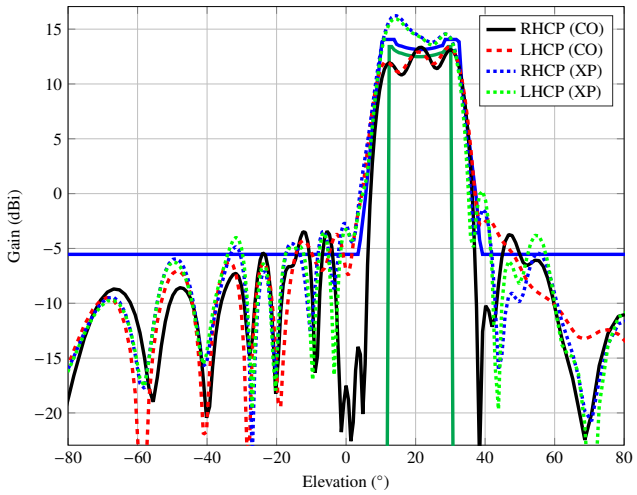

Fig. 5. Main cut in elevation of the copolar (CO) and crosspolar (XP) patterns at 18.5 GHz for RHCP and LHCP produced by the layout obtained after the POS.

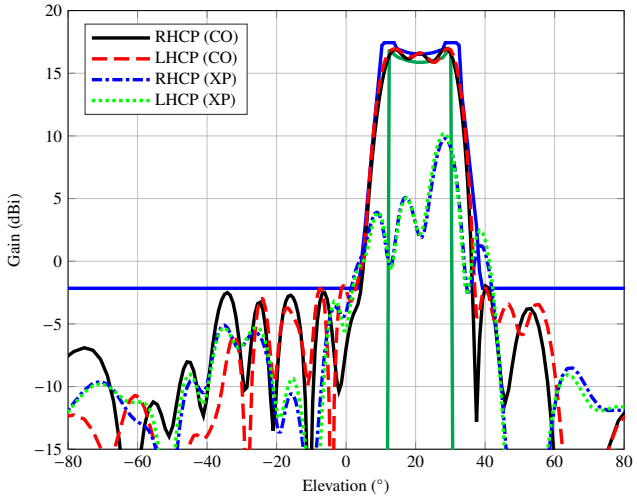

Fig. 6. Main cut in elevation at 18.5 GHz of the copolar (CO) and crosspolar (XP) patterns for RHCP and LHCP produced by the optimized layout taking into account only copolar requirements.

high, but also that the copolar pattern will be distorted due to the simplification in (19). These limitations will be tackled next by a direct layout optimization taking into account the full electromagnetic response of the unit cell.

D. Direct Layout Optimization

The POS step can be used as a starting point for a direct layout optimization, in which the length of the Jerusalem cross arms are the optimizing variables. The SVR models will be employed in this optimization, allowing to optimize both the copolar and crosspolar patterns simultaneously.

The GIA is employed for a direct layout optimization [17]. In order to facilitate convergence of the algorithm, the optimization will be carried out in two stages. First, a copolar-only direct optimization and, once the copolar pattern complies with the requirements, the crosspolar pattern will be minimized while preserving the copolar pattern within

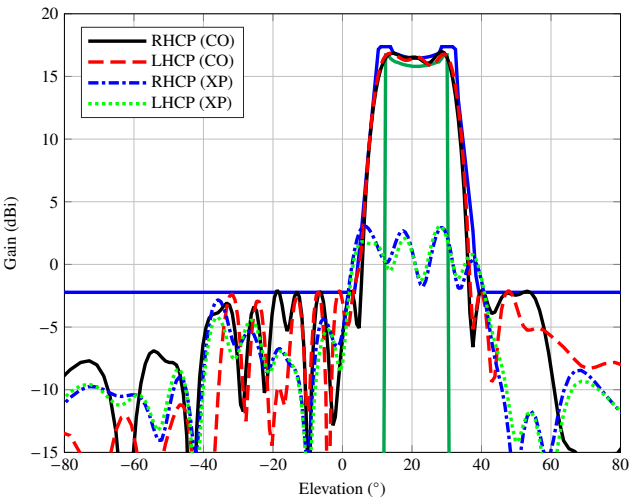

Fig. 7. Main cut in elevation at 18.5 GHz of the copolar (CO) and crosspolar (XP) patterns for RHCP and LHCP produced by the optimized layout taking into account both copolar and crosspolar requirements.

specifications. These two stages will be performed in three steps each, gradually increasing the number of variables. In the first step, only the length T_x will be optimized for all reflectarray elements at the same time. Then, T_y will be considered. Finally, both T_x and T_y will be optimized at the same time. In this way, the number of local minima is reduced and convergence improved.

Fig. 6 shows the main cut in elevation for both orthogonal polarizations produced by the optimized layout when only copolar requirements were considered. Now, the copolar pattern mostly lies within the upper and lower specification templates. It is also noticeable that, compared to Fig. 5, the gain has also improved around 4 dB. In addition, the maximum level of cross-polarization has been significantly reduced, from a maximum of 16.3 dBi in Fig. 5 to a maximum of 10.6 dBi in Fig. 6.

For the last stage in the optimization, cross-polarization requirements are included in addition to the copolar specifications. Specifically, the maximum level of the crosspolar pattern is to be minimized. Fig. 7 shows the radiation pattern obtained after this stage. The copolar pattern shape and gain are preserved while the maximum crosspolar level is further reduced from a maximum of 10.6 dBi in Fig. 6 to a maximum of 3.1 dBi now. This is a reduction of 7.5 dB between the two direct layout optimizations. With regard to the starting layout obtained after the POS, the total reduction in the crosspolar pattern is larger than 13 dB. In addition, the losses of the optimized antenna may be estimated by comparing the simulated gain shown in Fig. 7 and that of the shaped pattern in Fig. 4, which was obtained assuming ideal phase-shifters. The difference in gain in the coverage zone is around 1 dB, due to the losses introduced by the unit cell.

Fig. 8 shows full-wave simulations of the reflectarray with Ansys HFSS [19]. First, Fig. 8(a) compares, at the optimization frequency (18.5 GHz), the SVR-based simulation with that performed with HFSS. A small distortion in the coverage zone appears in the HFSS simulation, as well as an increase in the

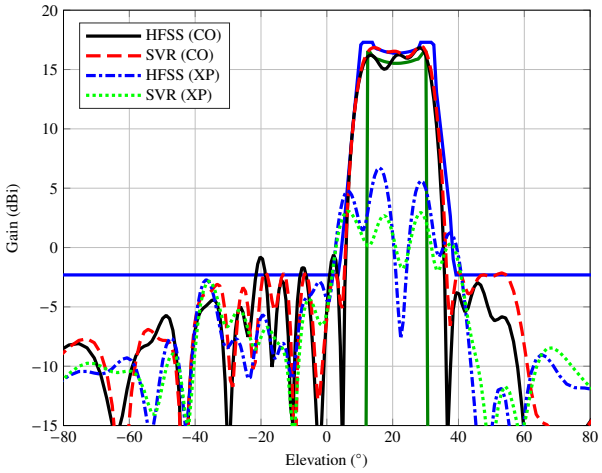

(a)

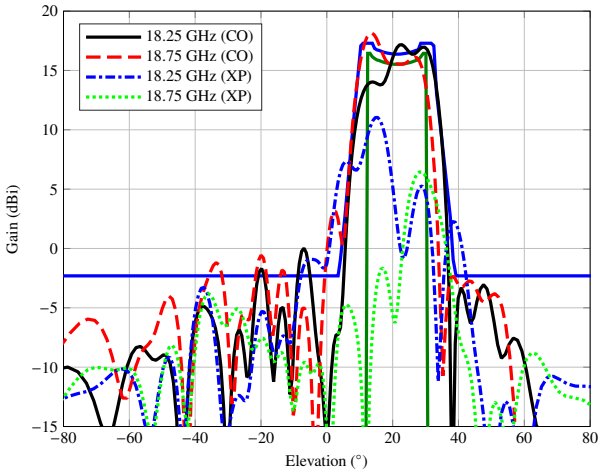

(b)

Fig. 8. Main cut in elevation of the copolar (CO) and crosspolar (XP) isoflux RHCP pattern comparing (a) HFSS and SVR-based simulations at 18.5 GHz, and (b) HFSS simulations at 18.25 GHz and 18.75 GHz.

crosspolar pattern of around 3.5 dB. Yet, the crosspolar pattern in the HFSS simulation is still more than 9 dB lower compared to the starting point of the optimization in Fig. 5, showing the effectiveness of the proposed methodology. Then, Fig. 8(b) shows HFSS simulations of the antenna at 18.25 GHz and 18.75 GHz. The copolar pattern is noticeably distorted while the maximum crosspolar pattern further increases its value. This shows the inherent narrow bandwidth of the reflectarray antenna [3] and the need for a multi-frequency optimization to achieve broadband behaviour. In this regard, although the methodology for the optimization of dual-CP shaped-beam reflectarrays has been shown for a single frequency, it can be extended to a broadband case by modifying the functional that is minimized in the backward projection of the GIA to include the radiation patterns at several frequencies [24], provided that the surrogate models are also available at other frequencies as well.

Table II
COMPUTATIONAL PERFORMANCE OF THE ANTENNA OPTIMIZATION PROCESS IF IT WERE CARRIED OUT WITH THE ANSYS HFSS SOFTWARE FOR THE CELL ANALYSIS. TOTAL TIME IS BASED ON AN AVERAGE UNIT CELL ANALYSIS TIME OF THREE MINUTES ON AN INTEL I9-9900 CPU.

		Total time (days)
Layout design	Phase-shift table	32
	N-R method	32
Direct layout optimization (CO-only)	Stage 1 (1024 DoF)	627
	Stage 2 (1024 DoF)	717
	Stage 3 (2048 DoF)	1709
Direct layout optimization (CO+XP)	Stage 1 (1024 DoF)	909
	Stage 2 (1024 DoF)	1651
	Stage 3 (2048 DoF)	2592
Overall process (no parallelization)		8269 (≈ 22.7 years)
Overall process (100% parallelization)		517 (≈ 1.4 years)
Overall process with SVR		33 minutes

E. Computational Performance

The main goal of employing SVR models of the unit cell is to substantially improve the computational performance of the overall optimization process. Although there is an initial cost of several days to generate the samples which will be employed in the training process, the subsequent use of the SVR models allows to save a considerable amount of time compared with the use of HFSS.

Fig. 3 shows the stages that are accelerated by the use of the SVR models. They are the layout design and the direct layout optimizations. The layout design has two stages that call the analysis routine: the generation of a phase-shift table and the Newton-Raphson (N-R) method. Assuming an average time of HFSS analysis of three minutes for each unit cell, and 15 calls for each stage (which is an underestimate of the total number of calls), it would take a total of 64 days to complete the layout design. However, using the SVR models it took less than three seconds.

The direct layout optimization is a heavier computational task. There are two building blocks that are accelerated by the use of the SVR models: the cost function and the computation of the Jacobian matrix [20]. In the cost function, all the elements are analysed once. In the computation of the Jacobian, there are as many columns as optimization variables, and only one element per column is analysed. In addition, each direct layout optimization is carried out in three stages, in the first two optimizing half the variables (either T_x or T_y for each element) and in the last stage all variables are optimized at the same time. In addition, each stage may run for a different number of iterations of the GIA, which uses three iterations of the Levenberg-Marquardt algorithm in the backward projection [17]. Taking all this into account, the direct layout optimization would take more than 8000 days (i.e., more than 20 years) to finish using HFSS.

Table II gathers all the information relating the estimated computational performance when using HFSS. Even when computations are parallelized assuming 100% parallelization efficiency, the antenna optimization would take more than a

year to complete. This strikingly contrasts with the use of SVR models, allowing to finish the process in less than an hour.

V. Conclusions

In this work we have developed the formulation to synthesize dual circular-polarized (CP) reflectarray antennas. The relations between the reflection coefficients in Cartesian and CP bases were derived. Then, it was proven that the copolar components of the far field in CP mainly depend on the direct reflection coefficients in CP basis provided a good performance of the feed and unit cell, allowing the phase-only synthesis (POS) of dual-CP reflectarray antennas. The formulation was then applied to the optimization of a shaped-beam dual-CP reflectarray with an isoflux pattern. Surrogate models based on support vector regression (SVR) were trained for their use in the optimization. The SVR models achieve a high degree of accuracy in the prediction of the reflection coefficients when compared with simulations with HFSS, while substantially improving computational performance.

The unit cell presents, however, some shortcomings: its total phase-shift for reflectarray design is limited to 300°, has high losses and high cross-polarization level. All these limitations may be overcome by a careful optimization process in several stages. Following this strategy, the optimized layout radiated an isoflux pattern in dual-CP that complies with the requirements in the copolar component while presenting an improved cross-polarization performance. Indeed, compared to the starting layout, the maximum cross-polarization level has been reduced more than 9 dB when simulating with HFSS, while improving the copolar shape and gain. These results show the robustness of the proposed methodology to design dual-CP reflectarrays with improved performance, which allows to relax performance constraints on the constituent unit cell.

Appendix

The far-field components are given by the application of Love's equivalence principle for aperture antennas [23]:

$$\begin{aligned} E_\theta &= A[P_x\cos\varphi + P_y\sin\varphi - \eta_0\cos\theta(Q_x\sin\varphi \\ &\quad - Q_y\cos\varphi)] \\ E_\varphi &= -A[\cos\theta(P_x\sin\varphi - P_y\cos\varphi) \\ &\quad + \eta_0(Q_x\cos\varphi + Q_y\sin\varphi)], \end{aligned} \tag{24}$$

where η_0 is the wave impedance of free space and:

$$A = \frac{jk_0\exp(-jk_0r)}{4\pi r}. \tag{25}$$

$P_{x/y}$ and $Q_{x/y}$ are obtained as the Fourier transform of the tangential fields at the reflectarray aperture:

$$\begin{aligned} P_{x/y} &= \iint_S E_{\mathrm{ref},x/y}(x,y)\exp(jk_0(ux+vy))dxdy, \\ Q_{x/y} &= \iint_S H_{\mathrm{ref},x/y}(x,y)\exp(jk_0(ux+vy))dxdy, \end{aligned} \tag{26}$$

where the subscript indicates the Cartesian component of the field according to the reflectarray coordinate system (see Fig. 1), S is the reflectarray surface, and (x, y) are the coordinates on the reflectarray surface. Eq. (26) can be efficiently computed with the fast Fourier transform algorithm [18].

With (24)–(26), the far field in CP is expressed as a function of the Cartesian spectrum functions $P_{x/y}$ and $Q_{x/y}$. However, it is possible to express the far field in CP as a function of a pair of CP spectrum functions. This will be useful for the demonstration of the POS formulation in CP. To that end, we substitute (24) into (13), obtaining:

$$\begin{aligned} E_{\mathrm{ff},r} &= A(B_1P_x + B_2P_y - j\eta_0B_1Q_x - j\eta_0B_2Q_y)/\sqrt{2}, \\ E_{\mathrm{ff},l} &= A(B_3P_x + B_4P_y + j\eta_0B_3Q_x + j\eta_0B_4Q_y)/\sqrt{2}, \end{aligned} \tag{27}$$

with:

$$\begin{aligned} B_1 &= \cos\varphi - j\cos\theta\sin\varphi, \\ B_2 &= \sin\varphi + j\cos\theta\cos\varphi, \\ B_3 &= \cos\varphi + j\cos\theta\sin\varphi, \\ B_4 &= \sin\varphi - j\cos\theta\cos\varphi. \end{aligned} \tag{28}$$

Next, we consider the definition of spectrum function P and Q from (26). For the electric field, we can obtain the Cartesian components as a function of the CP components from (7):

$$\begin{aligned} E_{\mathrm{ref},x} &= (E_{\mathrm{ref},r} + E_{\mathrm{ref},l})/\sqrt{2}, \\ E_{\mathrm{ref},y} &= -j(E_{\mathrm{ref},r} - E_{\mathrm{ref},l})/\sqrt{2}, \end{aligned} \tag{29}$$

and substituting (29) into (26) we arrive at:

$$\begin{aligned} P_x &= (P_r + P_l)/\sqrt{2}, \\ P_y &= j(-P_r + P_l)/\sqrt{2}, \end{aligned} \tag{30}$$

where P_r and P_l are defined in (14).

For Q, the reflected tangential magnetic field is needed. It is obtained with:

$$\vec{H}_{\mathrm{ref}} = \frac{\vec{k}_{\mathrm{ref}}\times\vec{E}_{\mathrm{ref}}}{\omega\mu_0}, \tag{31}$$

where $\omega = 2\pi f$, and:

$$\vec{k}_{\mathrm{ref}} = -k_0\sin\theta_i\cos\varphi_i\hat{x} - k_0\sin\theta_i\sin\varphi_i\hat{y} + k_0\cos\theta_i\hat{z}, \tag{32}$$

and (θ_i, φ_i) is the angle of incidence of the plane wave for the i-th reflectarray element (see Fig. 1). The $\hat{z}$ component of $\vec{E}_{\mathrm{ref}}$, necessary to solve (31), is obtained by solving the plane wave equation $\vec{E}_{\mathrm{ref}}\cdot\vec{k}_{\mathrm{ref}} = 0$. Then, the components of the reflected tangential magnetic field are:

$$\begin{aligned} H_{\mathrm{ref},x} &= -K_1E_{\mathrm{ref},x} - K_2E_{\mathrm{ref},y}, \\ H_{\mathrm{ref},y} &= K_3E_{\mathrm{ref},x} + K_1E_{\mathrm{ref},y}, \end{aligned} \tag{33}$$

with:

$$\begin{aligned} K_1 &= \frac{k_{\mathrm{ref},x}k_{\mathrm{ref},y}}{\omega\mu_0k_{\mathrm{ref},z}}, \\ K_2 &= \frac{k_{\mathrm{ref},y}^2 + k_{\mathrm{ref},z}^2}{\omega\mu_0k_{\mathrm{ref},z}}, \\ K_3 &= \frac{k_{\mathrm{ref},x}^2 + k_{\mathrm{ref},z}^2}{\omega\mu_0k_{\mathrm{ref},z}}. \end{aligned} \tag{34}$$

Now, substituting (29) into (33), we end up with:

$$\begin{aligned} H_{\mathrm{ref},x} &= (jK_2 - K_1)E_{\mathrm{ref},r}/\sqrt{2} - (K_1 + jK_2)E_{\mathrm{ref},l}/\sqrt{2}, \\ H_{\mathrm{ref},y} &= (K_3 - jK_1)E_{\mathrm{ref},r}/\sqrt{2} + (K_3 + jK_1)E_{\mathrm{ref},l}/\sqrt{2}, \end{aligned} \tag{35}$$

which in turn gives the following magnetic spectrum functions:

$$\begin{aligned} Q_x &= (jK_2 - K_1)P_r/\sqrt{2} - (K_1 + jK_2)P_l/\sqrt{2}, \\ Q_y &= (K_3 - jK_1)P_r/\sqrt{2} + (K_3 + jK_1)P_l/\sqrt{2}, \end{aligned} \tag{36}$$

Once the spectrum functions have been obtained, by substituting (30) and (36) into (27), the far field is finally written as:

$$\begin{aligned} E_{\mathrm{ff},r} &= C_1 P_r + C_2 P_l, \\ E_{\mathrm{ff},l} &= C_3 P_r + C_4 P_l, \end{aligned} \tag{37}$$

where:

$$\begin{aligned} C_1 &= A\{B_1 - jB_2 - j\eta_0[B_1(jK_2 - K_1) + B_2(K_3 - jK_1)]\}/2, \\ C_2 &= A\{B_1 + jB_2 + j\eta_0[B_1(K_1 + jK_2) - B_2(K_3 + jK_1)]\}/2, \\ C_3 &= A\{B_3 - jB_4 + j\eta_0[B_3(jK_2 - K_1) + B_4(K_3 - jK_1)]\}/2, \\ C_4 &= A\{B_3 + jB_4 - j\eta_0[B_3(K_1 + jK_2) - B_4(K_3 + jK_1)]\}/2. \end{aligned} \tag{38}$$

Please note that due to the relation between the reflected tangential electric and magnetic fields, $Q_{x/y}$ is expressed as a function of $P_{r/l}$ instead of an analogous $Q_{r/l}$ in (15), and thus it is not necessary to define $Q_{r/l}$ in the same way that $P_{r/l}$ was defined in (14).

REFERENCES

[1] S. Gao, Q. Luo, and F. Zhu, Eds., *Circularly Polarized Antennas*. Chichester, West Sussex, UK: John Wiley & Sons, 2012.

[2] C. A. Balanis, *Advanced engineering electromagnetics*. Hoboken, NJ, USA: John Wiley & Sons, 1989.

[3] J. Huang and J. A. Encinar, *Reflectarray Antennas*. Hoboken, NJ, USA: John Wiley & Sons, 2008.

[4] J. Huang and R. J. Pogorzelski, "Microstrip reflectarray with elements having variable rotation angles," in *Antennas and Propagation Society International Symposium*, vol. 2, Montreal, Quebec, Canada, Jul.13–18, 1997, pp. 1280–1283.

[5] V. F. Fusco, "Mechanical beam scanning reflectarray," *IEEE Trans. Antennas Propag.*, vol. 53, no. 11, pp. 3842–3844, Nov. 2005.

[6] Z. H. Jiang, T. Yue, and W. Hong, "Low-profile and wideband dual-circularly polarized reflect-arrays based on rotated metal-backed dual-polarized aperture-coupled patch elements," *IEEE Trans. Antennas Propag.*, vol. 68, no. 3, pp. 2108–2117, Mar. 2020.

[7] M. R. Chaharmir and J. Shaker, "Design of a multilayer X-/Ka-band frequency-selective surface-backed reflectarray for satellite applications," *IEEE Trans. Antennas Propag.*, vol. 63, no. 4, pp. 1255–1262, Apr. 2015.

[8] E. Martinez-de-Rioja *et al.*, "Advanced multibeam antenna configurations based on reflectarrays: Providing multispot coverage with a smaller number of apertures for satellite communications in the K and Ka bands," *IEEE Antennas Propag. Mag.*, vol. 61, no. 5, pp. 77–86, Oct. 2019.

[9] M. Zhou, S. B. Sørensen, Y. Brand, and G. Toso, "Doubly curved reflectarray for dual-band multiple spot beam communication satellites," *IEEE Trans. Antennas Propag.*, vol. 68, no. 3, pp. 2087–2096, Mar. 2020.

[10] P. Naseri, M. Riel, Y. Demers, and S. V. Hum, "A dual-band dual-circularly polarized reflectarray for K/Ka-band space applications," *IEEE Trans. Antennas Propag.*, vol. 68, no. 6, pp. 4627–4637, Jun. 2020.

[11] D. Martinez-de-Rioja, R. Florencio, E. Martinez-de-Rioja, M. Arrebola, J. A. Encinar, and R. R. Boix, "Dual-band reflectarray to generate two spaced beams in orthogonal circular polarization by variable rotation technique," *IEEE Trans. Antennas Propag.*, vol. 68, no. 6, pp. 4617–4626, Jun. 2020.

[12] X. Tong, Z. H. Jiang, Y. Li, F. Wu, R. Sauleau, and W. Hong, "Dual-wideband dual-circularly-polarized shared-aperture reflectarrays with a single functional substrate for K-/Ka-band applications," *IEEE Trans. Antennas Propag.*, 2022, early access.

[13] M. Karimipour, N. Komjani, A. Abdolali, and S. Abbaszade, "Optimum design of dual band shaped-beam circularly polarized reflectarray antenna based on physical optic method," *Int. J. RF Microw. Comput. Eng.*, vol. 26, no. 8, pp. 690–702, Oct. 2016.

[14] S. V. Polenga *et al.*, "A Ka-band shaped-beam circularly polarized reflectarray antenna," in *Radiation and Scattering of Electromagnetic Waves (RSEMW)*, Divnomorskoe, Russia, Jun. 24–28, 2019, pp. 281–284.

[15] V. Richard *et al.*, "Spherical mapping of the second-order phoenix cell for unbounded direct reflectarray copolar optimization," *Progr. Electromagn. Res. C*, vol. 90, pp. 109–124, 2019.

[16] M. Arrebola, J. A. Encinar, and M. Barba, "Multifed printed reflectarray with three simultaneous shaped beams for LMDS central station antenna," *IEEE Trans. Antennas Propag.*, vol. 56, no. 6, pp. 1518–1527, Jun. 2008.

[17] D. R. Prado *et al.*, "Efficient crosspolar optimization of shaped-beam dual-polarized reflectarrays using full-wave analysis for the antenna element characterization," *IEEE Trans. Antennas Propag.*, vol. 65, no. 2, pp. 623–635, Feb. 2017.

[18] D. R. Prado, M. Arrebola, M. R. Pino, and F. Las-Heras, "Complex reflection coefficient synthesis applied to dual-polarized reflectarrays with cross-polar requirements," *IEEE Trans. Antennas Propag.*, vol. 63, no. 9, pp. 3897–3907, Sep. 2015.

[19] "HFSS," Ansys Inc., Pittsburgh, Pennsylvania, USA.

[20] D. R. Prado, J. A. López-Fernández, M. Arrebola, M. R. Pino, and G. Goussetis, "General framework for the efficient optimization of reflectarray antennas for contoured beam space applications," *IEEE Access*, vol. 6, pp. 72 295–72 310, 2018.

[21] C.-C. Chang and C.-J. Lin, "LIBSVM: A library for support vector machines," *ACM Trans. Intell. Syst. Technol.*, vol. 2, no. 3, pp. 27:1–27:27, Apr. 2011, software available at https://www.csie.ntu.edu.tw/~cjlin/libsvm.

[22] D. R. Prado, J. A. López-Fernández, G. Barquero, M. Arrebola, and F. Las-Heras, "Fast and accurate modeling of dual-polarized reflectarray unit cells using support vector machines," *IEEE Trans. Antennas Propag.*, vol. 66, no. 3, pp. 1258–1270, Mar. 2018.

[23] W. L. Stutzman and G. A. Thiele, *Antenna Theory and Design*, 3rd ed. Hoboken, NJ, USA: John Wiley & Sons, 2012.

[24] D. R. Prado, J. A. López-Fernández, M. Arrebola, M. R. Pino, and G. Goussetis, "Wideband shaped-beam reflectarray design using support vector regression analysis," *IEEE Antennas Wireless Propag. Lett.*, vol. 18, no. 11, pp. 2287–2291, Nov. 2019.

Daniel R. Prado was born in Sama de Langreo, Asturias, Spain, in 1986. He received the B.Sc., M.Sc., and Ph.D. degrees in telecommunication engineering from the University of Oviedo, Gijón, Spain, in 2011, 2012, and 2016, respectively.

From 2010 to 2011, he was with The Institute of Electronics, Communications and Information Technology, Queen's University Belfast, Belfast, U.K., where he was involved in the design of leaky-wave antennas as part of his B.Sc. research project. From 2011 to 2017, he was a Research Assistant with the Signal Theory and Communications Area, University of Oviedo, where he was involved in the development of efficient techniques for the analysis and synthesis of reflectarray antennas. In 2014, he was with the School of Electrical Engineering, KTH Royal Institute of Technology, Stockholm, Sweden, as a Visiting Scholar, where he was involved in transformation optics applied to dielectric lenses. From 2018 to 2019, he was with the Institute of Sensors, Signals and Systems, Heriot-Watt University, Edinburgh, U.K. Since 2020 he has been with the Signal Theory and Communications Area, University of Oviedo, as a Post-doctoral researcher. His current research interests include the analysis of uniform and nonuniform arrays, and the development of efficient techniques for the analysis and optimization of near and far fields of spatially-fed antennas, including reflectarrays and transmitarrays.

Dr. Prado was a recipient of a Pre-doctoral Scholarship financed by the Gobierno del Principado de Asturias, a Post-doctoral Fellowship partially financed by the European Union and a Post-doctoral Fellowship financed by the Spanish Government.

Parinaz Naseri (Graduate Student Member, IEEE) received the B.Sc. degree from the University of Tehran, Tehran, Iran, in 2013, and the M.Sc. degree from the University of Alberta, Edmonton, AB, Canada, in 2017, both in electrical and computer engineering. She is currently pursuing the Ph.D. degree with the University of Toronto (UofT), Toronto, ON, Canada.

In 2018, she joined The Edward S. Rogers Senior Department of Electrical and Computer Engineering, UofT, as a Researcher, where she is conducting research on the design of electromagnetic surfaces for space applications using machine learning techniques. She also serves as the Lab Manager for the Reconfigurable Antenna Laboratory, UofT.

Ms. Naseri was a recipient of the Stanley G. Jones Master's Scholarship in 2014, the Prestigious Ontario Trillium Scholarship in 2018, the Donald R. Studney Electromagnetics Graduate Award in 2020, and the Prestigious IEEE Antenna and Propagation Society Doctoral Research Grant in 2021. She was a recipient of a Research Grant at the Instituto de Telecomunicacoes, Lisbon, Portugal, in 2016, to work on European Space Agency-funded projects on metasurface-based solutions for satellite communications, from 2016 to 2018. She has been the Organizer and Chair of the IEEE AP-S Student Branch Chapter, UofT, since October 2020. She also serves as a Technical Reviewer for a number of journals and conferences including the IEEE TRANSACTIONS ON ANTENNAS AND PROPAGATION, the *Open Journal of Antennas and Propagation*, and the European Conference on Antennas and Propagation.

Jesús Alberto López-Fernández was born in Avilés, Asturias, Spain. He received the M.Sc. and Ph.D. degrees in telecommunication engineering from the University of Vigo, Vigo, Spain, in 1999 and 2009, respectively.

From April 2002 to March 2003, he was a Marie-Curie Visiting Fellow with the Mechanical & Manufacturing Engineering Department, Trinity College Dublin. Since October 2003, he has been with the Electrical Engineering Department, University of Oviedo, Asturias, Spain, where he is currently an Associate Professor teaching courses on digital communications and radar systems. His current research interests include iterative methods and speed-up schemes, parallel algorithms, machine learning and signal processing.

Sean Victor Hum (Senior Member, IEEE) received the B.Sc., M.Sc., and Ph.D. degrees in electrical and computer engineering from the University of Calgary, Calgary, AB, Canada, in 1999, 2001, and 2006, respectively.

In 2006, he joined The Edward S. Rogers Senior Department of Electrical and Computer Engineering, University of Toronto (UofT), Toronto, ON, Canada, where he is currently a Professor and the Eugene V. Polistuk Chair in electromagnetic design. He was the Associate Chair, Graduate Studies with the same department, from 2018 to 2021. He leads the Reconfigurable Antenna Laboratory, UofT, and along with his students, conducts research in the areas of advanced electromagnetic surfaces, reconfigurable/multifunction antennas, space-fed arrays, and antennas for space applications.

Dr. Hum was a recipient of the Governor General's Gold Medal for his work on radio-on-fiber systems in 2001, the IEEE Antennas and Propagation Society Student Paper Award for his work on electronically tunable reflectarrays in 2004, the ASTech Leaders of Tomorrow Award for his work in this area in 2006, the Early Researcher Award from the Government of Ontario in 2012. On the teaching side, he has been the recipient of several departmental teaching awards and a Faculty Early Career Teaching Award. He was a co-recipient of the IEEE Antennas and Propagation Society R. W. P. King Award in 2015 and 2017. He served on the Steering Committee and the Technical Program Committee of the 2010 and 2020 IEEE AP-S International Symposium on Antennas and Propagation. He was the TPC Co-Chair of the 2015 IEEE AP-S International Symposium on Antennas and Propagation. He served as an Associate Editor for the IEEE TRANSACTIONS ON ANTENNAS AND PROPAGATION from 2010 to 2017. He is currently Co-Chair of the IEEE AP-S Education Committee.

Manuel Arrebola (Senior Member, IEEE) was born in Lucena, Córdoba, Spain. He received the M.Sc. degree in telecommunication engineering from the University of Málaga, Málaga, Spain, in 2002, and the Ph.D. degree from the Technical University of Madrid (UPM), Madrid, Spain, in 2008.

From 2003 to 2007, he was a Research Assistant with the Department of Electromagnetism and Circuit Theory, UPM. In 2005, he was a Visiting Scholar with the Department of Microwave Techniques, Universität Ulm, Ulm, Germany. In 2007, he joined the Department of Electrical Engineering, University of Oviedo at Gijón, Spain, where he is currently an Associate Professor. In 2009, he was with the European Space Research and Technology Centre, European Space Agency, Noordwijk, The Netherlands, for a period of two months. In 2018, he was a Visiting Professor with the Edward S. Rogers Sr. Department of Electrical and Computer Engineering, University of Toronto, Toronto, ON, Canada. In 2019, he was a Visiting Professor with the Institute of Sensors, Signals and Systems, Heriot-Watt University, Edinburgh, U.K. His current research interests include the development of efficient analysis, design, and optimization techniques of reflectarray and transtmitarray antennas both in near- and far-fields.

Dr. Arrebola was a co-recipient of the 2007 S. A. Schelkunoff Transactions Prize Paper Award given by the IEEE Antennas and Propagation Society.